Mechanics of Composite Materials and Structures, 7:269–284, 2000
Copyright © 2000 Taylor & Francis
1075-9417/00 $12.00 + .00

Prediction of Buckling-Mode Interaction in Composite Columns

EVER J. BARBERO

West Virginia University, Morgantown, West Virginia, USA

ABSTRACT

Pultruded structural shapes are often used as columns of intermediate length, for which the global and local buckling loads are close. Interaction between the two buckling modes is accounted for in design by an empirical interaction constant. Theoretical/numerical prediction of such a constant is presented in this article. Stability theory is used to demonstrate the existence of buckling-mode interaction. The continuation method is used to study the imperfection sensitivity of the columns. A relationship between column imperfection and the interaction constant is established. Experimental results are presented to support the analysis.

Most columns made of polymer matrix composites (PMC) are produced by pultrusion, in which case they are called structural shapes. The manufacturers [14, 24, 28] offer a broad selection of geometry and materials. They are used because of their high strength-to-weight ratio, resistance to environmental deterioration, and lack of interference with electromagnetic radiation. Since composite columns are thin-walled, buckling is a major consideration in design. Two types of column failure modes are well known. Local (flange) buckling dominates the behavior of stubby columns. Global (Euler) buckling controls the behavior of slender columns. For intermediate lengths, the local and global buckling modes interact, leading to smaller failure loads than predicted by any of the two isolated modes acting alone [29, chap. 12]. In design, the interactive behavior for intermediate-length columns is taken into account by an empirical constant [6]. Prediction of such constant as a function of geometry, materials properties, and imperfections of the column is the object of this investigation. For metallic columns the interaction takes place between one buckling mode and yield, but composites remain linear for large strains, thus allowing for the interaction between different buckling modes.

Local buckling occurs in short columns that are long enough not to fail due to crushing, that is, when the compression strength of the material is not reached [8, 11, 13]. For pultruded wide-flange (WF) sections as shown in Figure 1, the column will compress axially until flanges develop wavelike deformations along the length. The flange deformations can be large, often greater than the thickness of the flanges. The short column buckling load P_L can be determined from a short column test [10, 30] or predicted using analytical or numerical

Received 23 September 1999; accepted 6 January 2000.

This project was sponsored by West Virginia Division of Highways contract RP #131, and National Science Foundation grant CMS-9612162. The financial support is appreciated.

Address correspondence to Ever J. Barbero, 315 Engineering Science Building, West Virginia University, Morgantown, WV 26506-6106. E-mail: ebarbero@wvu.edu

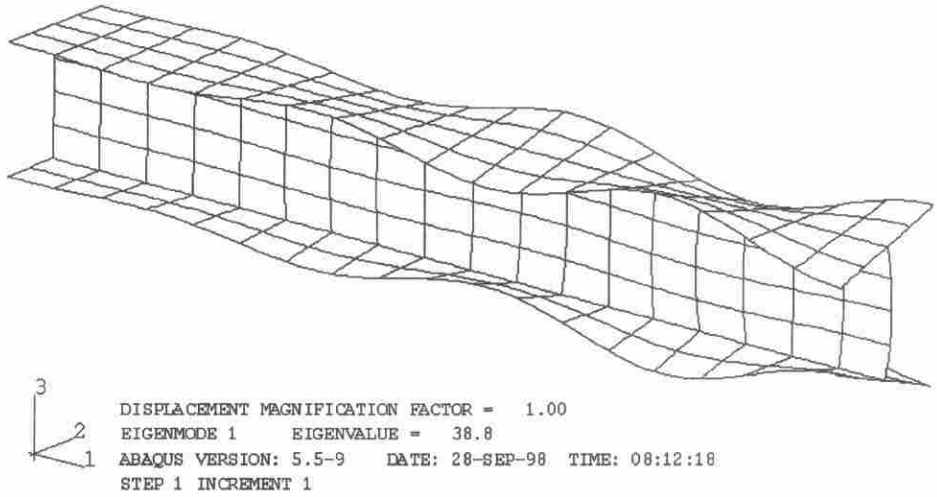

Figure 1. *Sample geometry, coordinate system, and deformations of the local buckling mode.*

techniques [3–5, 16, 17, 23, 31, 32, etc.]. Its value is independent of the length of the column as long as the column is short and wave amplitude modulation [22] is not a factor.

The global (Euler) mode occurs in slender columns and involves a sudden lateral deflection without deformation of the cross section (Figure 2). The Euler buckling equation,

$$P_E = \frac{EI}{(kL/\pi)^2} \tag{1}$$

accurately predicts the critical buckling load for slender columns in terms of the bending stiffness (EI), the column length L, and the end-restraint coefficient k. As pointed out by Gaylord and Gaylord [19], the reduction of buckling load due to shear deformation can be accounted for by dividing the result of Eq. (1) by $1 + P_E/(GA)$, where (GA) is the shear

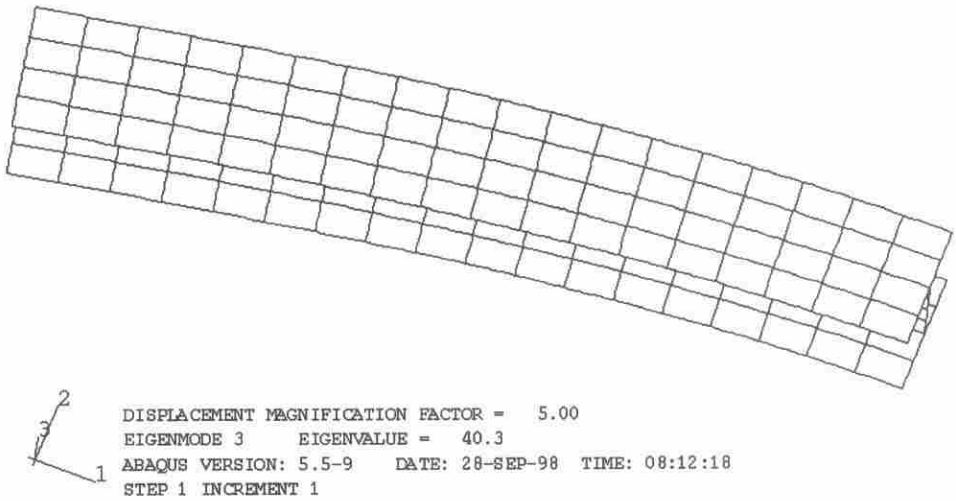

Figure 2. *Euler buckling mode.*

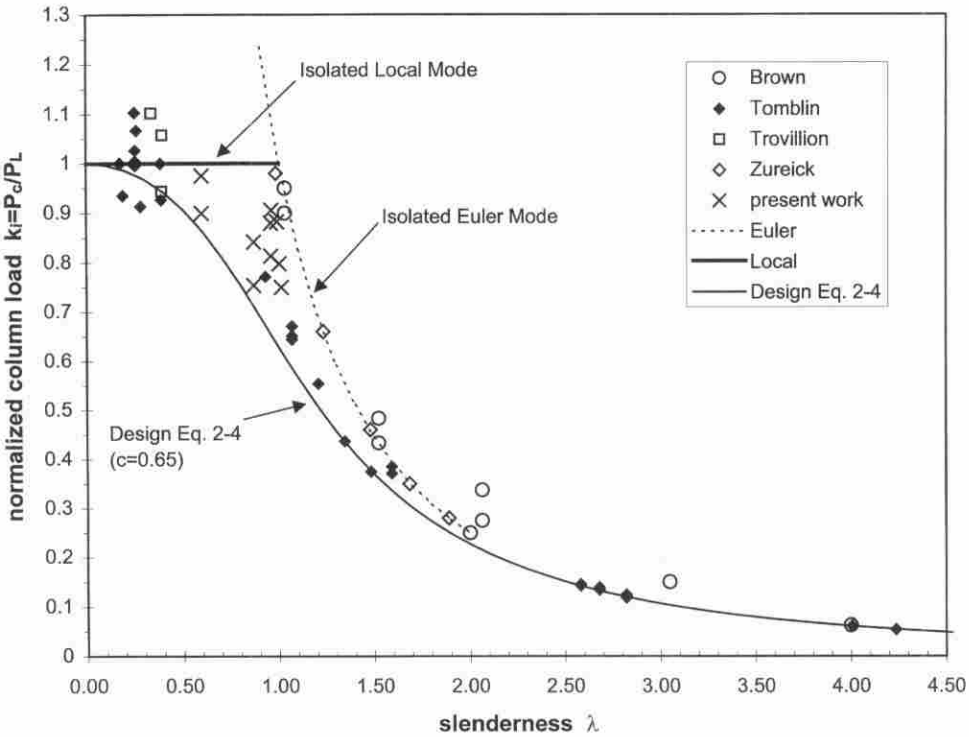

Figure 3. *Column experimental data and predictions by various equations used in design.*

stiffness of the cross section, given by Barbero [9], section 8.2.7 for open cross sections and 8.2.8 for closed cross sections.

When the length of the column is such that the predicted local and global loads are close, the experimental failure load is lower than both predictions, depending on the imperfections. This was shown experimentally by Barbero and Tomblin [6] and by Barbero et al. [12] for columns, and by Foster [18] for shells. An empirical equation was proposed by Barbero and Tomblin [6] to model the data from the literature (see Figure 3). According to the empirical equation, the column-buckling load is predicted as

$$P_c = k_i P_L \tag{2}$$

where P_L is the short-column load, and the resistance factor k_i in Eq. (2) due to mode interaction is

$$k_i = k_\lambda - \sqrt{k_\lambda^2 - \frac{1}{c\lambda^2}} \tag{3}$$

where $k_\lambda = (1 + 1/\lambda^2)/2c$ is a coefficient introduced for convenience; c is the empirical interaction constant adjusted to fit the data, and λ is the composite slenderness, defined as

$$\lambda = \frac{kL}{\pi}\sqrt{\frac{P_L}{(EI)}} \tag{4}$$

The bending stiffness (EI) can be measured from a bending test [2] or back-calculated from a slender-column test using Eq. (1). The main objective of this article is to provide a method to predict the interaction constant c, which so far has had to be determined from column tests [6, 12].

FE MODELING

Finite-element modeling provides the engineer with a powerful tool that consistently predicts the physical behavior of a particular structural member without having to conduct numerous laboratory tests. In most situations, only one buckling mode is considered at any given time. This is called isolated-mode analysis, and is the easiest to perform. However, the experimental results of Barbero and Tomblin [6] and Barbero et al. [12] have shown that two or more buckling modes can act coincidentally at certain lengths for thin-walled pultruded columns. Therefore, a finite-element procedure that can predict the buckling behavior of intermediate-length columns is needed.

In this work, the buckling and postbuckling were modeled using perturbation techniques [7] and continuation methods [1]. Identical material properties and boundary conditions were used in both analyses. The numerical results were compared with experimental results. For stubby and slender columns, it was found that the finite-element model closely predicted the bifurcation load and the curvature of the postcritical path, as long as the local and Euler bifurcation loads where far apart. For intermediate-length columns, it was found that a linear combination of the isolated modes (local and Euler) could predict a deformation field similar to the experimental deformation data.

A nine-node Lagrangian element was used to model the column [7]. The geometry of the column was discretized into 18 elements along the length, 4 elements across the width of the flange, and 4 elements across the height of the web (Figure 1) for a total of 216 elements and 925 nodes. From a convergence study (Figure 4), it was found that this

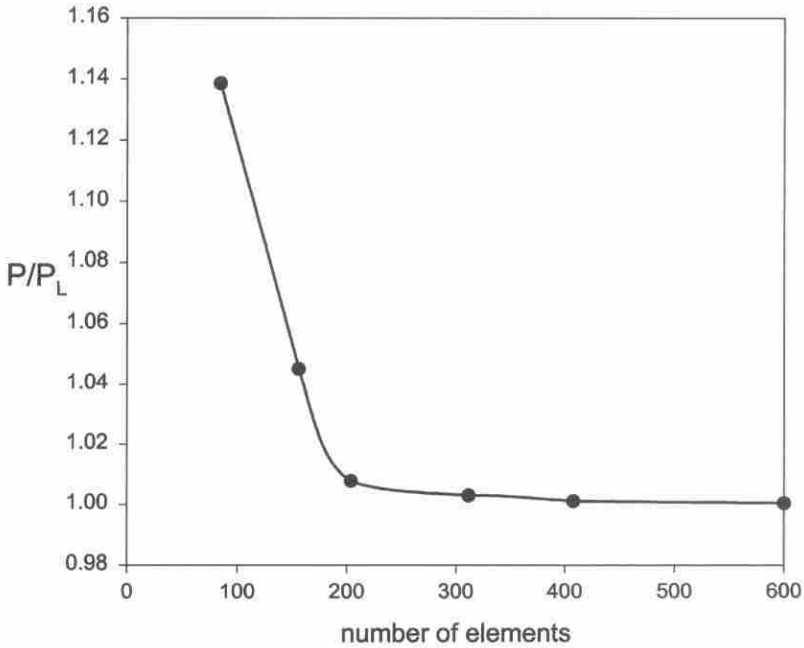

Figure 4. *FE mesh convergence.*

Table 1
Stiffness coefficients of the 152 × 152 × 6.35 mm (web 7.14 mm) structural shape

	Flange		Web	
Component	A (MPa mm)	D (MPa mm^3)	A (MPa mm)	D (MPa mm^3)
11	163,370	489,226	158,176	767,573
12	31,996	116,521	32,038	152,831
22	87,165	308,006	88,103	420,500
66	25,649	91,080	26,132	124,985
44	15,788	0	16,378	0
55	15,338	0	15,955	0

provided a reasonable balance between accuracy and computational expense. The material properties for the elements are given in terms of the coefficients of the stiffness matrices ($[A_{ij}]$ and $[D_{ij}]$) reported in Table 1.

The boundary conditions were applied by constraining the displacements of the nodes at the end of the column and using symmetry at the mid-span. Multipoint constraints were used to keep the end cross section undeformed and flat but allowing it to rotate around the z axis, which coincides with the z direction. Boundary conditions were used to model the pinned-pinned end conditions with respect to the weak axis. To simulate the clamping effect of the grips, the rotation around the y axis of all the flange nodes was constrained. This introduces wave modulation; that is, the amplitude of the buckling shape is reduced near the supports. This effect was observed in the experiments. The column was loaded by applying a distributed compressive load in the x direction to the web nodes. All results are normalized with respect to the short-column buckling load P_L.

Perturbation analysis

The objective of this section is to find the bifurcation points and draw the equilibrium paths of the perfect system (Figure 5). This type of analysis reveals the asymptotic behavior of the structure, as the imperfections become negligible. Imperfection sensitivity and mode interaction of the structure can be assessed without having to choose a particular imperfection shape and amplitude, as is required in continuation methods. Thus, the results of the analysis of the perfect system are general.

To illustrate the perturbation analysis, let us consider a 152 × 152 × 6.35 mm, 2.18 m long WF column. It has been proposed [7, 21] that buckling-mode interaction can be modeled as the linear combination of the local, Euler, and a third buckling mode. For the example considered, the lowest bifurcation load corresponds to the local buckling mode. Since the column length modeled was close to the interaction length, the Euler mode is close to the local mode load.

A third isolated mode must be included in the analysis because a combination of only two modes is not capable of modeling interaction, as shown by Raftoyiannis et al. [25]. Any number of buckling modes may interact with the local and Euler buckling modes. The only criteria available for the selection of the third isolated mode are (1) it must be different from the local and Euler modes, (2) it leads to an interacting path (which may be unstable), and (3) the resulting interacting mode resembles the mode shape observed in the experiments. For a new problem for which the postcritical behavior is not known, we

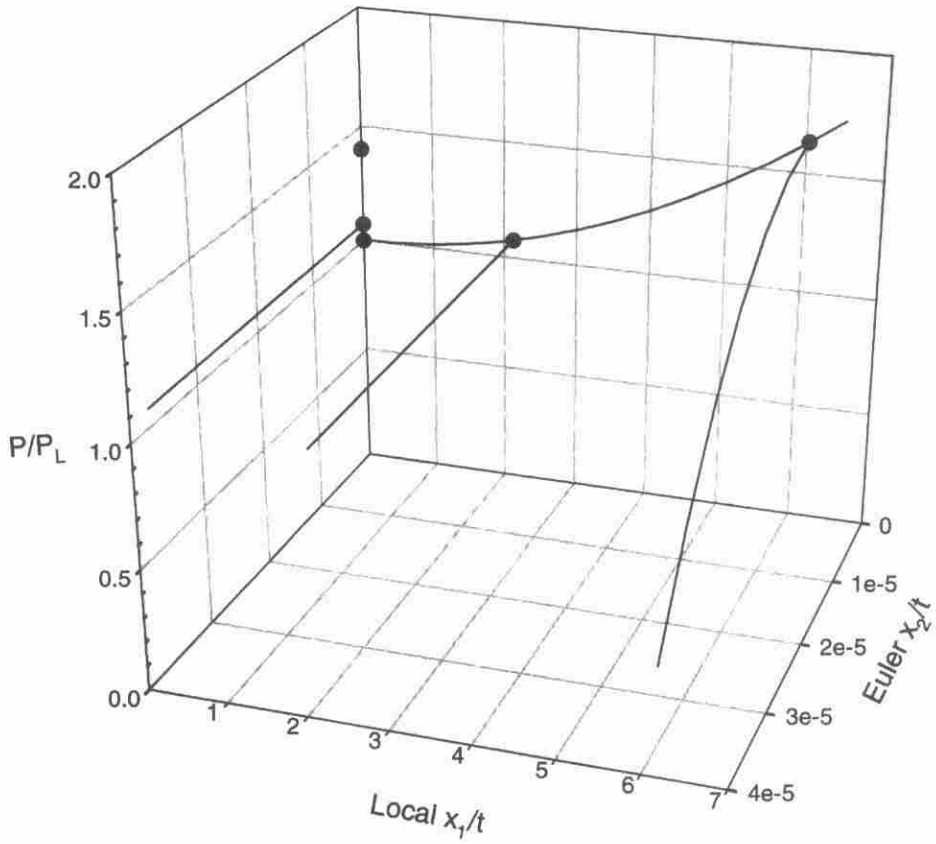

Figure 5. *Stability of the perfect system.*

conclude that there is interaction if any of the available third modes ($N-2$ of them) leads to a tertiary (interacting) path.

Once the three buckling modes for which buckling-mode interaction is to be investigated have been selected, the resulting buckling shape must be determined. It was proposed by Barbero et al. [7] that the nodal displacements in the original FE model can be written as a linear combination of the three interacting modes (reduced space expansion), as

$$a_i = x_i^1 \xi_1 + x_i^2 \xi_2 + x_i^3 \xi_3 \tag{5}$$

where x_i^j are the nodal displacement vectors ($i = 1, \ldots, N$; $j = 1, 2, 3$) for a particular mode ($j = 1$, local; $j = 2$, Euler; $j = 3$, third mode), ξ_j are modal amplitudes (i.e., scalars), and a_i are the resulting nodal displacements. Substituting Eq. (5) into the equilibrium equation (Eqs. 14–16 in [7]), we obtain a new equilibrium equation in terms of the nodal displacements (x_i^j) and modal amplitudes ξ_j as

$$\left(\Lambda - \Lambda_c^s\right)\delta_{st}\xi_t + A^{stu}\xi_t\xi_u + B^{stuv}\xi_t\xi_u\xi_v = 0 \tag{6}$$

where $s, t, u, v = 1, 2, 3$; Λ is the load parameter, Λ_c^s is the critical load of the mode s, and A^{stu} is given by

$$A^{stu} = F^{stu} + \Lambda G^{stu} \tag{7}$$

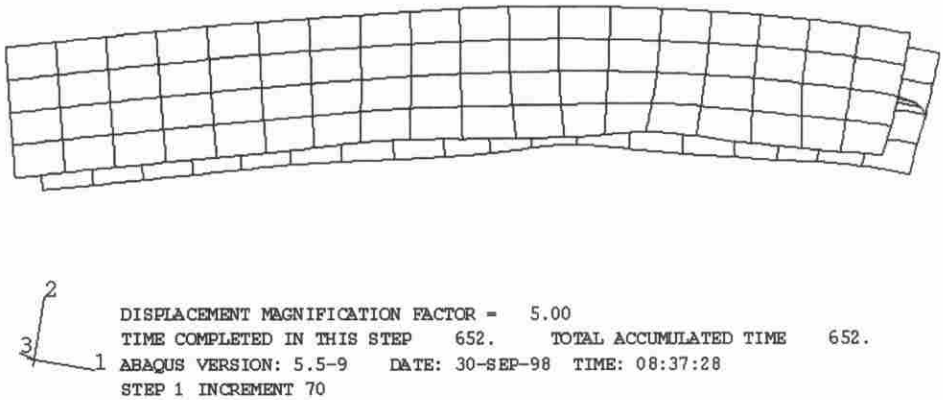

Figure 6. *Interacting buckling mode.*

and the interaction coefficients F^{stu} and G^{stu} are computed by the FE perturbation program [15]. The solution of the modal amplitudes ξ_i was also done using perturbation techniques.

A single root of Eq. (6) must be picked in order to determine the proper mode amplitudes ξ_j for buckling-mode interaction. The chosen root should be on the postcritical path, at a reasonable load. The most efficient way of choosing the proper bifurcation point was to plot all roots as in Figure 5, where x_1 is the displacement of the tip of the flange at the mid-span, x_2 is the lateral (Euler) displacement of the column at the mid-span, P is the load, and P_L is the lowest bifurcation load (in this case corresponding to the local mode). The primary path is trivial, with $x_1 = x_2 = 0$. There are three bifurcation points on the load axis, which are simply the bifurcations for the isolated modes. There are two secondary paths, both of which are stable and symmetric. The lowest bifurcation and path corresponds to the local mode, the next one to the Euler mode. Note that the Euler path is very shallow as opposed to the local path, which has a noticeable curvature.

There are two bifurcations on the secondary local path. The first yields a stable tertiary path similar to the Euler mode; the second yields an unstable tertiary path. The unstable path deformations have components in both x_1 and x_2, as can be seen in Figure 5. Therefore, the tertiary path is a different mode shape resulting from the interaction between the local and Euler modes, as can be seen also in Figure 6. Note that the tertiary path results from the interaction between the local and Euler modes when both bifurcation loads are close. If these loads are far apart, no tertiary path appears and the structure is insensitive to imperfections.

Since the tertiary path is unstable, the behavior of a real, imperfect column will be imperfection-sensitive, and failure will be catastrophic, with no load capacity after buckling. Imperfection sensitivity means that the peak or failure load of the imperfect system will be lower than the bifurcation load of the perfect system; the magnitude of the reduction depends on the magnitude of the imperfection. Therefore, a continuation method will be used later to evaluate the peak load.

Experimental Results

The buckling-mode interaction tests were performed on a horizontal buckling frame described by Barbero and Tomblin [6]. All specimens were 152 × 152 × 6.35-mm pultruded WF columns provided by Creative Pultrusions, Inc. The specimens were prepared using a band saw to cut the ends squarely with respect to the flange surface. The columns were mounted in the frame in such a manner as to have one of the flange surfaces facing upward, so that gravity acts on the strong axis, which is not tested. Therefore, gravity does not

contribute to the Euler buckling mode. Mounted to the inside of the adjustable and the movable crosshead were two shoes with pin-and-needle bearings, which provide the pinned-pinned end conditions for the test. The load and stroke were measured using a load cell and internal LVDT mounted on the actuator. Another LVDT was attached to the side of the sample to measure Euler-type deformations. The shadow moiré optical technique [26] was used to measure out-of-plane displacements of the top flange. Since this is a noncontact technique, the development of the buckling mode is unaffected by the instrumentation. Video acquisition was used to record the moiré image and the digital values of stroke, load, and lateral displacements into a composite image on a VCR. This composite image can later be captured, frame by frame, from the SVHS VCR using the video acquisition software. The image is then digitized, the initial fringe readings are subtracted, and the result is shown as a contour plot.

The contour plot obtained by moiré measures out-of-plane displacements $\delta(x, y)$ of the flange. Thus, it provides only the evolution of the local mode. Since the Euler mode causes deflections parallel to the plane of the flange, the Euler deformations cannot be seen on the fringe pattern. Therefore, an LVDT was mounted to record the Euler mode. Since the flange deflection δ can be measured everywhere on the flange, for all times, a decision has to be made of what numerical values to report. Here, the numerical values reported are the maximum deflections, which occur at the tip of the flanges, at the mid-span. This information was used to compute the curvature $\Lambda^{(2)}$ of the postcritical path. Furthermore, the moiré data were used along with the Southwell method [27, 30] to compute the buckling loads $P_{\exp}$ reported in Table 2.

Ten specimens were prepared from the available WF columns to various lengths, shown in Table 2. The test was run at a stroke rate of at 2.5 mm/min, which was slow enough to observe the growth of the fringe pattern, yet provided reasonable test duration for taping purposes. All columns had surface imperfections that caused initial fringes to appear. When processing the data, these initial fringes are subtracted from the overall fringe orders obtained throughout the duration of the test. The compression side of the column had more fringe

Table 2

Comparison of bifurcation loads and postcritical curvature with experimental results

Sample number	Slenderness, λ	$P_{\exp}/P_{\text{bif}}$[a]	Curvature, Λ_2 exp. (1/cm^2)	Curvature, Λ_2 pert. (1/cm^2)	% diff.
1	0.824	1.029	1.083	0.767	−29%
2	0.868	1.041	0.996	0.785	−21%
3	0.868	0.753	0.689	0.785	14%
4	0.868	0.840	1.093	0.785	−28%
5	0.957	0.878	1.242	0.865	−30%
6	0.959	0.812	1.924	0.865	−55%
7	0.960	0.904	0.566	0.865	53%
8	0.991	0.881	1.024	0.819	−20%
9	1.002	0.797	1.195	0.855	−28%
10	1.013	0.768	NA	0.787	

[a] P_{bif} indicates the lowest bifurcation load, either local or Euler mode.

patterns than the tension side as buckling developed in the intermediate-length columns. Along with the increased number of fringe patterns, a lower wavelength was observed on the compression side. No twisting of the column was observed.

The bifurcation loads P_{bif} were determined by calculating the y intercept of the imaginary line P–δ^2, where P is the measured load and δ^2 is the measured flange displacement squared. The curvature of the postcritical path $\Lambda^{(2)}$ is computed as the slope of the line P–δ^2 divided by the bifurcation load P_{bif}. The experimental bifurcation loads P_{bif} and the corresponding postcritical path curvatures $\Lambda^{(2)}$ were determined for both the more and less compressive flange displacement data (indicated by δ^+ and δ^-) for each column length tested. The two experimental values were averaged and reported in Table 2.

For each length tested, the bifurcation loads and the curvature of the post critical path $\Lambda^{(2)}$ were compared with the finite-element results. The perturbation program predicts a bifurcation into a local mode for stubby columns (slenderness $\lambda < 1$) and a bifurcation load into an Euler mode for slender columns ($\lambda > 1$). The bifurcation load was for a local mode at $P_L = 170$ kN for all columns except for the sample with $\lambda = 1.013$, which had a bifurcation into an Euler mode at $P_E = 165.7$ kN. The experimental results show lower ultimate loads $P_{\text{exp}}/P_{\text{bif}}$ as λ increases, as shown in Table 2.

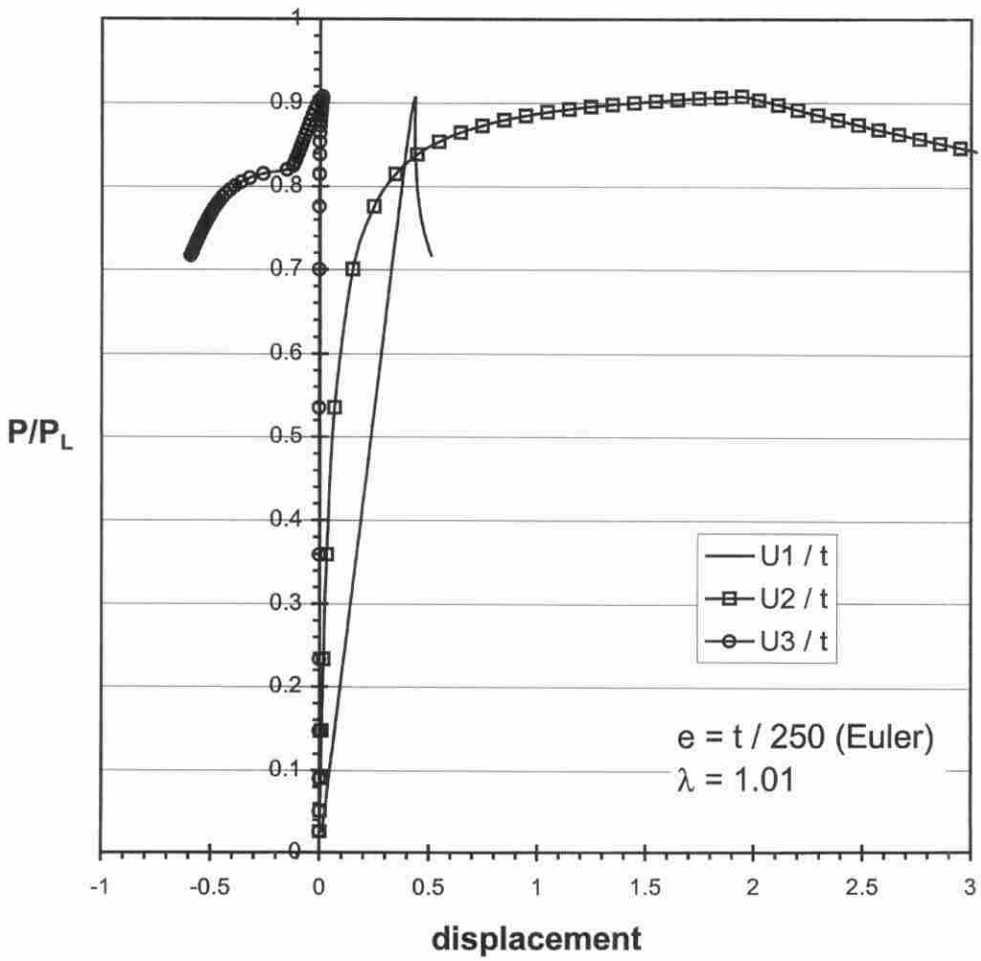

Figure 7. *Continuation solution for the imperfect system.*

From Table 2 it can be seen that the experimental and numerical values of curvature $\Lambda^{(2)}$ do not agree closely, nor is there any clear pattern of disagreement. This is due to the coupling of the two near-coincident buckling modes (local and Euler). The coupling of two or more buckling modes causes the postbuckling behavior to develop into a tertiary mode that is different from the isolated-local mode. Since the experimental postcritical path curvature ($\Lambda^{(2)}$ exp.) were calculated from actual deformations and the theoretical postcritical path curvature ($\Lambda^{(2)}$ pert.) were calculated for the isolated buckling mode, it can be concluded that the numerical results of isolated-mode analysis do not present an accurate picture of the actual postcritical behavior. This is further indication of the development of an interacting mode shape different from the isolated-local mode.

DETERMINATION OF THE INTERACTION CONSTANT

Columns of intermediate length are those that have close values of Euler and local bifurcation (buckling) loads. Using stability theory and a perturbation analysis of the perfect system, it was shown above that the proximity of two isolated buckling modes (local and Euler) yields a tertiary unstable path. Therefore, columns of intermediate length are imperfection-sensitive, with a maximum load that is lower than the bifurcation load of either

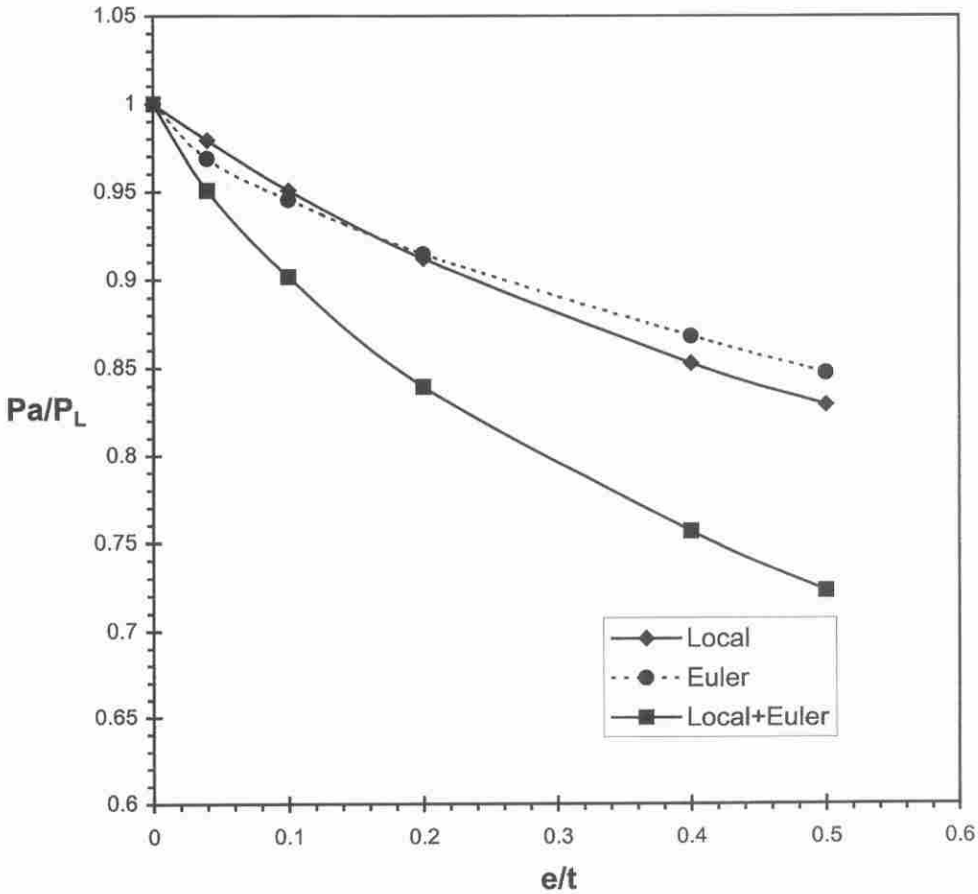

Figure 8. *Effect of imperfection shape.*

one of the isolated modes (Euler or local). The maximum load that can be applied to the column is a function of the amplitude of the imperfection. Therefore, a continuation method was used to study the effect of imperfections. The column was modeled with Abaqus including geometric nonlinearity, and the nonlinear system was solved using the Riks method [1]. A shell element S9R5 was used in Abaqus.

Three types of imperfections were applied, an imperfection in the form of either local or Euler mode, and a combination of both. Material inhomogeneities, twist, and deviations in thickness in the flanges and web are other sources of imperfection which have a bearing on buckling, but these are difficult to measure and it is believed that their effect would be similar to that induced by other geometric imperfections. The amplitude of the imperfections used in this work spanned the interval $t/250$ to $t/2$, where t is the thickness of the flange. The range of slenderness spanned the interval 0.7 to 1.25. The unstable postbuckling behavior is illustrated clearly in Figure 7 for a column of critical length; the critical length L_{CR} is the length for which the Euler and local bifurcations occur at the same load ($\lambda = 1$). Note that the behavior is highly unstable on the axial displacement U1 (stroke) and the flange displacement U3. During test, it was observed that the intermediate column is so unstable that the compliance of the sample and test fixture is sufficient to overcome the servo-control that tries to impose a controlled displacement (stroke). All intermediate-length tests conducted yielded catastrophic failures.

The FE model results indicate that any imperfection shape induces instability. For example, an imperfection with the shape of the Euler mode induced instability on columns

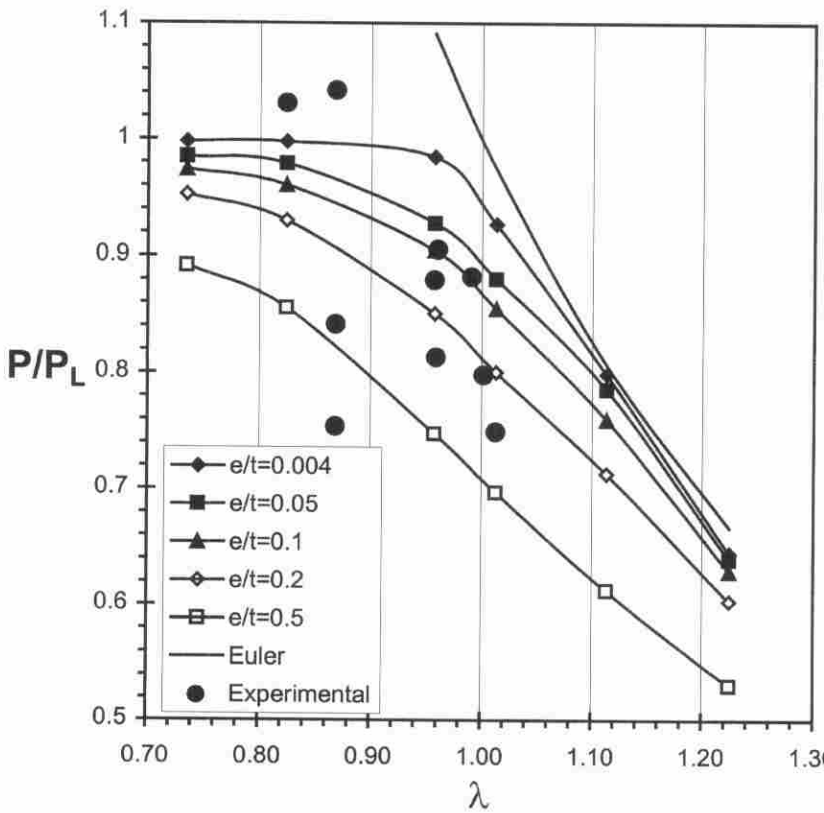

Figure 9. *Effect of imperfection amplitude* e/t.

shorter or longer than the critical length. The same happened if the imperfection shape was that of the local mode or a combination of both. This is emphasized in Figure 8, where the imperfection sensitivity curve is shown for the three cases; namely, the imperfection is in the shape of the local mode, Euler mode, or a combination of both. Note that the local and Euler imperfections produce virtually the same curve. A combination of both imperfections causes more reduction in load simply because the effect of both imperfections add up; the two imperfections act like a single, larger one.

As shown in Figure 7, even with a small imperfection ($e = t/250$), the peak load drops about 10% when the slenderness is $\lambda = 1.01$. Form the experimental as well as numerical results we conclude that the reduction of peak load is a function of slenderness and imperfection amplitude, but not of imperfection shape.

The effect of slenderness is shown in Figure 9, where symbols indicate different imperfections amplitudes e/t. With a very small imperfection (0.004) the behavior approaches the two isolated modes, local for $\lambda < 1$ and Euler for $\lambda > 1$. The interactive behavior is remarkable for all other values of imperfection. The experimental data shown in Figure 9 have significant scatter because each point represents a different sample, with different imperfection. However, the data agree well with the trend predicted by the numerical results.

The effect of the imperfection amplitude can be observed in the imperfection sensitivity plot in Figure 10, for various constant values of slenderness (indicated by symbols). The larger the imperfection, the larger is the reduction of the peak load. However, slenderness does play a role by magnifying the reduction.

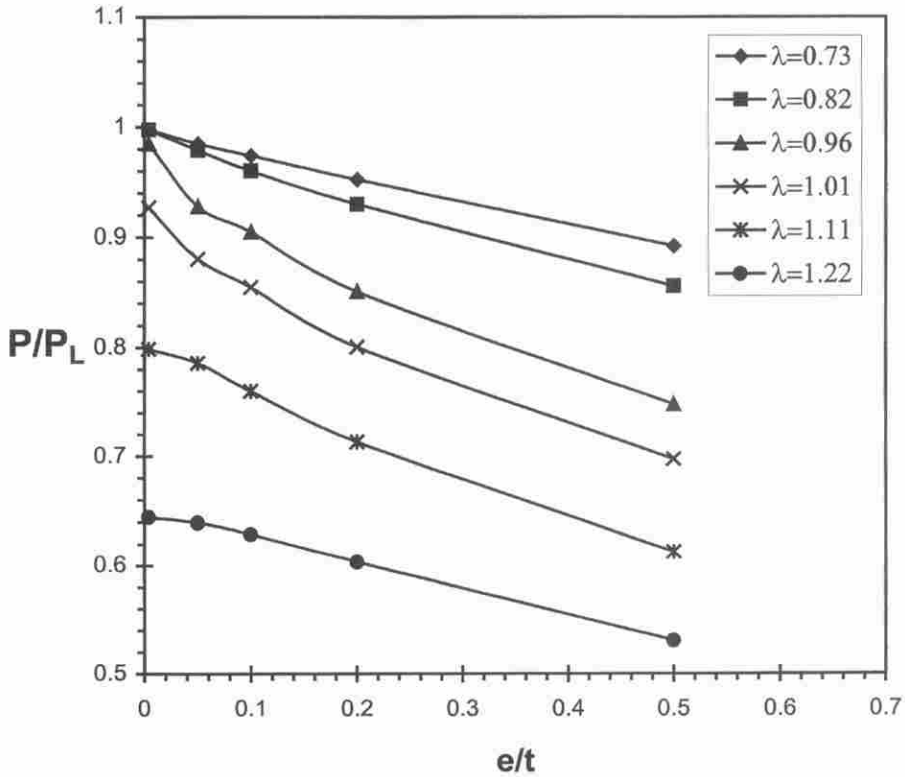

Figure 10. *Effect of slenderness* λ.

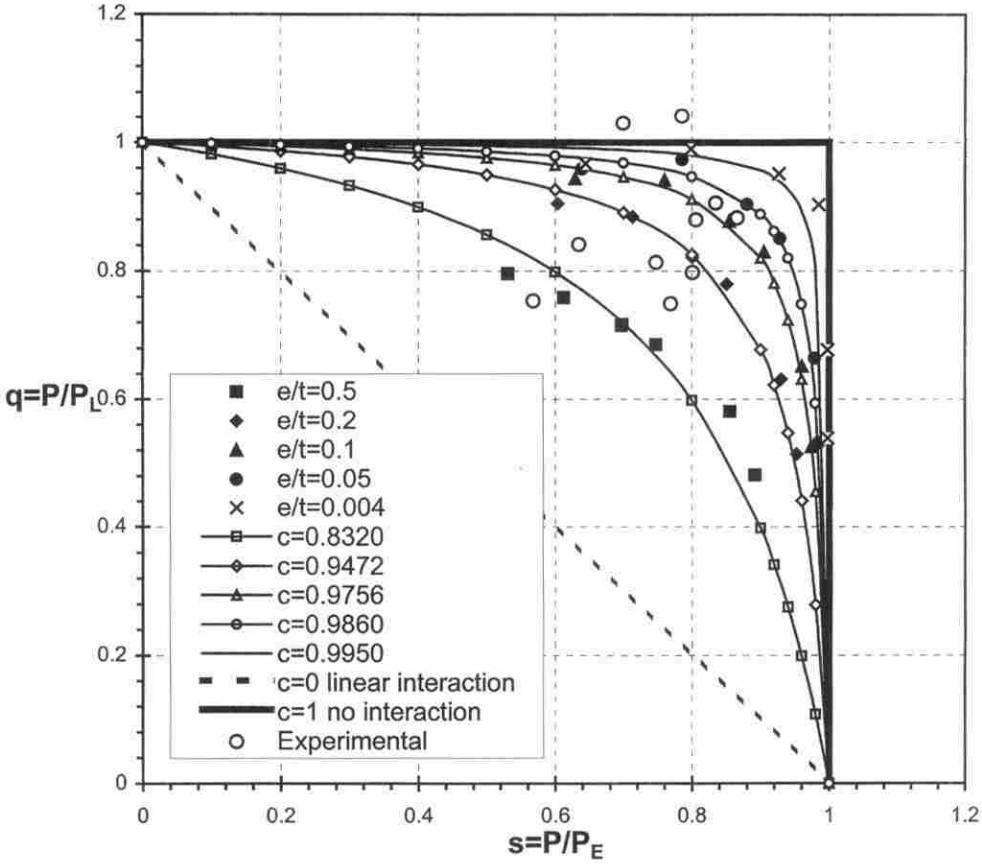

Figure 11. *Interaction plot.*

Plots like Figure 11 are called interaction plots, and they are commonly used in design. Here the peak load is normalized by the isolated local bifurcation load ($q = P/P_L$) and by the isolated Euler bifurcation load ($s = P/P_E$). This type of graph is very useful in that it clearly shows the deviation of the peak load from each isolated mode prediction, local and Euler. The case of no interaction ($c = 1$) is represented by a square delineated by $q = 1$ on the top and $s = 1$ on the right. Linear interaction between the two modes (local and Euler) is given by the diagonal line, and this is often used in design as a conservative estimate, although in certain problems it may not be conservative [20]. The solid symbols represent peak loads from the numerical simulation for various values of imperfection amplitude (indicated in the legend). For each imperfection amplitude, several points represent different values of slenderness. For each value of imperfection amplitude, the simulation data were fitted with the empirical interaction equation [6].

$$q + s = 1 + cqs \tag{8}$$

which models interaction by an adjustable constant c. In the past, this constant could be found only from experimental data, but here it is found from simulation data. The lines with symbols represent the best fit to the data for each imperfection amplitude, and the corresponding values of c are given in the legend. Note that this process accounts for the

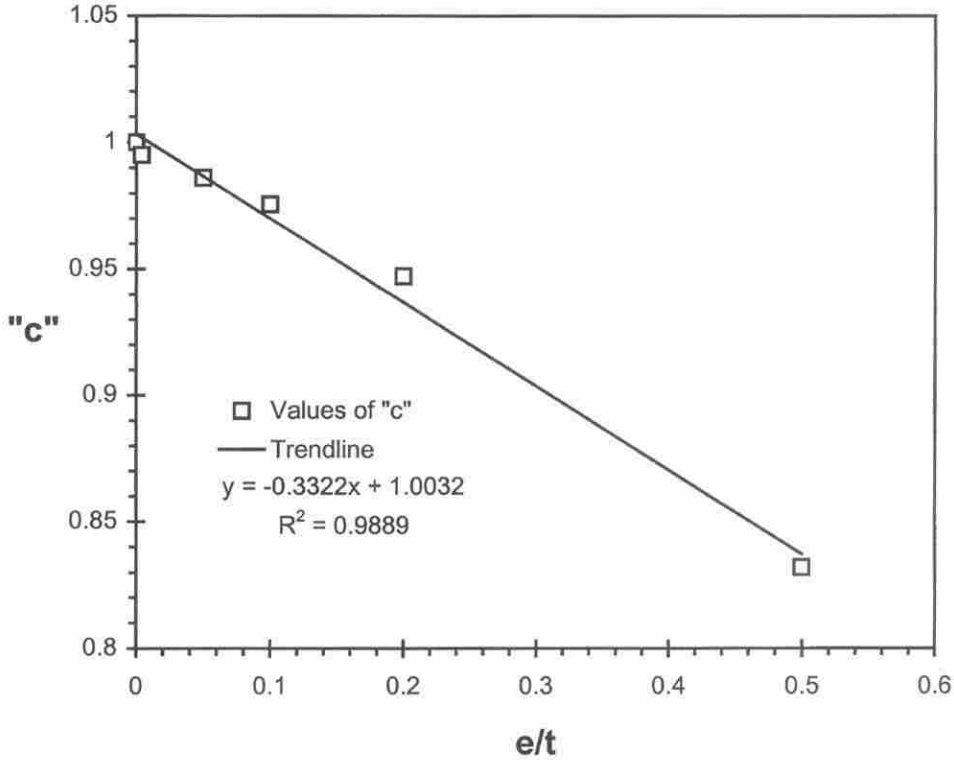

Figure 12. *Effect of imperfection on the interaction constant* c.

effect of slenderness because all the data for various slenderness values is represented by a single value of c corresponding to a given imperfection amplitude. Then, we see that Eq. (8) fits quite well the data for various values of slenderness. Experimental data is represented by open circles in Figure 11.

This process is appealing from a design point of view because the designer does not need to be concerned by the effect of slenderness, since it is automatically taken into account by Eq. (8). The only remaining variable is the magnitude of the imperfection. Values of c taken from the best fit to the data in Figure 11 are shown in Figure 12 versus slenderness. As can be seen in Figure 12, the effect of the imperfection amplitude e/t can be represented very well by a linear equation,

$$c = 1 - 0.3322(e/t) \tag{9}$$

Once the designer estimates the imperfection amplitude (e/t), Eq. (9) yields c, and Eqs. (2)–(4) can be used to compute the peak load for any slenderness value called for in the design. For design purposes, an estimate of the imperfection amplitude can be obtained from the geometric tolerances reported by the manufacturers. Specifically, the maximum camber of crookedness of columns is reported in product literature as a function of the column length [14, 24, 28].

Conclusions

An analysis of the stability of the perfect system demonstrates that the proximity of local and global buckling modes results in new interacting modes, some of which are unstable. The stability of the interacting modes leads to imperfection sensitivity, which is

confirmed by a continuation analysis. The experimental data also confirm the sensitivity to imperfections and the effect of slenderness as predicted by the analysis. The effect of slenderness is accurately captured by the design equations (2)–(4) in terms of an interaction constant c, as shown in the interaction plot. The imperfection shape is shown not to have any significant influence on the behavior. On the other hand, the imperfection magnitude has a linear effect on c, thus leading to a simple design equation (9). Therefore, Eqs. (2)–(4) and (9) can be used for the design of structures made with composite columns in the whole range of slenderness from stubby to intermediate to long columns. The methodology presented in this work can be used to obtain the interaction constant c, which is used in the design equations. Predicting the interaction behavior is very important for the development of new structural shapes, since production of prototype samples is very expensive in the pultrusion process because of the cost of the dies and guiding system. Furthermore, hundreds of commercially available structural shapes could be analyzed as proposed herein, thus limiting any experimental program to the verification of the proposed methodology instead of performing costly experimentation for all the shapes.

References

[1] *Abaqus Theory Manual*, HKS, Pawtucket, RI, 1998.

[2] L. C. Bank, Flexural and Shear Moduli of Full-Section Fiber Reinforced Plastic (FRP) Pultruded Beams, *J. Testing Eval.*, vol. 17, no. 1, pp. 40–45, 1989.

[3] L. C. Bank and J. Yin, Buckling of Orthotropic Plates with Free and Rotationally Restrained Unloaded Edges, *Thin-Walled Struct.*, vol. 24, pp. 83–96, 1996.

[4] W. M. Banks and J. Rhodes, The Instability of Composite Sections, *2nd Int. Conf. on Composite Structures*, Paisley, UK, pp. 442–452, Elsevier, Amsterdam, 1983.

[5] E. J. Barbero and I. Raftoyiannis, Buckling Analysis of Pultruded Composite Columns, in D. Hui (ed.), *Impact and Buckling of Structures*, ASME AD-Vol. 20, AMD-Vol. 114, pp. 47–52, 1990.

[6] E. J. Barbero and J. Tomblin, A Phenomenological Design Equation for FRP Columns with Interaction between Local and Global Buckling, *Thin-Walled Struct.*, vol. 18, pp. 117–131, 1994.

[7] E. J. Barbero, L. A. Godoy, and I. Raftoyiannis, Finite Elements for Three-Mode Interaction in Buckling Analysis, I, *J. Numer. Meth. Eng.*, vol. 39, pp. 469–488, 1996.

[8] E. J. Barbero, Prediction of Compression Strength of Unidirectional Polymer Matrix Composites, *J. Composite Mater.*, vol. 32, no. 5, pp. 483–502, 1998.

[9] E. J. Barbero, *Introduction to Composite Materials Design*, Taylor & Francis, Philadelphia, 1998.

[10] E. Barbero and J. Trovillion, Prediction and Measurement of the Post-Critical Behavior of Fiber-Reinforced Composite Columns, special issue on Civil Infrastructural Applications of Composite Materials, vol. 58, no. 8, pp. 1335–1441, 1998.

[11] E. J. Barbero, S. Makkapati, and J. S. Tomblin, Experimental Determination of Compressive Strength of Pultruded Structural Shapes, *Composite Sci. Technol.*, vol. 59, pp. 2047–2054, 1999.

[12] E. J. Barbero, E. Dede, and S. Jones, Experimental Verification of Buckling-Mode Interaction in Intermediate-Length Composite Columns, I, *J. Solid Struct.*, 1999.

[13] E. J. Barbero and E. A. Wen, Compressive Strength of Production Parts without Compression Testing, *ASTM STP 1383, Composite Structures: Theory and Practice*, ASTM, Philadelphia, 2000.

[14] *Bedford RP Design Guide*, Bedford Reinforced Plastics, Bedford, PA, 1993.

[15] BMI3, Three-Mode Buckling Mode Interaction Software, 1998, http://www.cemr.wvu.edu/~ejb/software.html.

[16] N. D. Brown, J. T. Mottram, and D. Anderson, The Behavior of Columns for the Design of Pultruded Frames: Tests on Isolated Centrally Loaded Columns, *2nd Int. Conf. on Composities in Infrastructure*, Tucson, AZ, vol. 2, pp. 248–260, 1998.

[17] J. F. Davalos and P. Qiao, Engineering Design Analysis Equations for Local Buckling of FRP Structural Shapes, *2nd Int. Conf. on Composites in Infrastructure*, Tucson, AZ, vol. 2, pp. 248–260, 1998.

[18] C. G. Foster, Interaction of Buckling Modes in Thin-Walled Cylinders, *Exp. Mech.*, vol. 21, no. 3, pp. 124–128, 1981.

[19] E. H. Gaylord and L. N. Gaylord, *Design of Steel Structures*, 2d ed., McGraw-Hill, New York, 1972.

[20] L. A. Godoy, S. R. Idelsohn, and E. J. Barbero, On Load Interaction in the Non-Linear Buckling Analysis of Cylindrical Shells, *Adv. Eng. Software TN*, vol. 13, no. 1, pp. 46–50, 1991.

[21] L. A. Godoy, E. J. Barbero, and I. Raftoyiannis, Interactive Buckling Analysis of Fiber-Reinforced Thin-Walled Columns, *J. Composite Mater.*, vol. 29, no. 5, pp. 591–613, 1995.

[22] L. A. Godoy, *Theory of Stability*, Taylor & Francis, Philadelphia, 1999.

[23] M. Pecce, F. Lazzaro, and E. Cosenza, Local Buckling of FRP Profiles: Experimental Results and Numerical Analyses, *European Conf. on Composite Materials*, Napoli, Italy, ECCM-8, pp. 331–338, 1998.

[24] *Pultex Design Guide*, Creative Pultrusions, Alum Bank, PA, 1989.

[25] I. Raftoyiannis, L. A. Godoy, and E. J. Barbero, Buckling Mode Interaction in Composite Plate Assemblies, *Appl. Mech. Rev.*, vol. 48 (11, part 2), pp. 52–60, 1995.

[26] R. C. Schwarz, Determination of Out-of-Plane Displacements and the Initiation of Buckling in Composite Structural Elements, *Exp. Techn.* pp. 23–28, 1988.

[27] R. V. Southwell, On the Analysis of Experimental Observations in Problems of Elastic Stability, *Proc. R. Soc. Lond. (A)*, vol. 135, pp. 601–616, 1932.

[28] *Strongwell Design Manual*, Strongwell, Bristol, VA, 1994.

[29] J. M. T. Thompson and G. W. Hunt, *A General Theory of Elastic Stability*, Wiley, London, 1973.

[30] J. Tomblin and E. J. Barbero, Local Buckling Experiments on FRP Columns, *Thin-Walled Struct.*, vol. 18, pp. 97–116, 1991.

[31] S. Vakiener, A. Zureick, and K. M. Will, Prediction of Local Flange Buckling in Pultruded Shapes by Finite Element Analysis, in *Advanced Composite Materials*, pp. 310–312, ASCE, New York, 1991.

[32] R. L. Yuan, Z. Hashen, A. Green, and T. Bisarnsin, Fiber-Reinforced Plastic Composite Columns, in S. L. Iyer (ed.), *Advanced Composite Materials in Civil Engineering Structures*, pp. 205–211, ASCE, Las Vegas, NV, 31 Jan.–1 Feb. 1991.